Probability of Error and Capacity of Multipolarization Antenna Systems for Downlink Mobile Communications

Yan Zhou, *Student Member, IEEE,* and Akbar M. Sayeed, *Senior Member, IEEE*

***Abstract*—A theoretical channel model is proposed to study the probability of error and channel capacity of multipolarization antenna systems for downlink mobile communications. The effect of scattering on polarization is first studied based on Fresnel reflection law. Expressions for correlation between antennas at both sides are derived for different polarizations. To simplify the analysis, it is assumed that there is only a single reflection and the path angular spread at the base station is approximately zero. Next, the probability of error and channel capacity are studied numerically for different antenna configurations. The impact of scattering environment on performance is also investigated. It is found that when a three-branch orthogonal structure is used for diversity at the mobile station, the error probability is invariant to receiver orientations, and the improvement is insignificant for more receive antennas. At the base station, both probability of error and channel capacity are substantially improved by using two transmit antennas that produce orthogonal polarizations in the direction of the mobile station, and the performance is invariant to rotations of the two transmit antennas. In addition, for almost all configurations, the performance becomes better in general for larger angular spread of reflectors.**

***Index Terms*—Channel capacity, mobile communications, polarization diversity.**

I. Introduction

THE POLARIZATION of an electromagnetic wave has been studied over several decades and also has many applications in wireless communications. For instance, two orthogonal polarizations have been utilized in microwave and satellite communication systems for orthogonal transmission, while they are usually used for diversity reception in mobile communications. One major advantage of polarization diversity is its low cost and complexity, since only two colocated antennas with orthogonal polarizations are required. Therefore, it is especially suitable for mobile handsets, in which space is normally limited. Numerous measurement campaigns have been conducted to assess the performance of polarization diversity in the uplink [3], [6], [9], [10], [13], [19]. The branch correlation and mean power difference were measured in [3] and [9] when vertical and horizontal polarizations are used for diversity, while the results for a $\pm 45^{\circ}$ slanted antenna configuration can be found in [6]. Measurement was further extended to the case of 1.8 GHz transmission [13], [19], and polarization diversity was also compared with other diversity methods in indoor environments [10]. On the other hand, the downlink counterpart seems to have received disproportionately little attention, and to the authors' knowledge, the corresponding literature is not plentiful [8], [25], [28], [29]. Both vertical/horizontal and $\pm 45^{\circ}$ configurations were compared in [25] and [28], while the performance of a three-branch orthogonal structure was evaluated in [29].

Most of the work on performance assessment of polarization diversity is based on measurements, which strongly depend on the environment, and excessive measurements in various environments are impractical. Theoretical studies are indispensable to get a comprehensive and complementary understanding of diversity performance. In addition, as previously mentioned, most research has been aimed at performance in the uplink. Polarization diversity is more desirable at the mobile station, where the space is much more limited. This motivates the theoretical analysis of polarization diversity in the downlink. On the other hand, channel capacity of multiple-input-multiple-output (MIMO) systems have become an important research area in recent years [17], [20], [23]. Multiple antennnas are employed on both sides to construct several parallel channels, which can greatly enhance the data rate for a given bandwidth. The channel capacity can also be increased by using colocated multipolarization antennas. This paper considers MIMO systems with multipolarization antennas at both sides and studies two key performance metrics: probability of error and channel capacity, which quantify the diversity advantage, and the maximum information rate of the system. The overall goal of this work is to evaluate the performance improvement achieved by different polarization configurations and to determine the most efficient configuration for a given scattering environment.

The remainder of this paper is organized as follows. In Section II, the effect of scattering on polarization is studied based on Fresnel reflection law [7], which has been verified in realistic mobile radio environments [14]. Expressions for correlation between transmit/receive antennas are then derived for different polarizations. In Section III, the probability of error and channel capacity are studied numerically for different antenna configurations. Through analysis, the performance relationship between different configurations is investigated. Relation to existing work is described in Section IV, and concluding remarks are presented in Section V.

Manuscript received July 29, 2002; revised November 26, 2003, January 27, 2004, August 24, 2004, and March 1, 2005. This work was supported by NSF Grant CCR-0113385. The review of this paper was coordinated by Dr. K. Dandekar.

The authors are with the Department of Electrical and Computer Engineering, University of Wisconsin-Madison, Madison, WI 53706 USA (e-mail: yanz@cae.wisc.edu; akbar@dune.ece.wisc.edu).

Digital Object Identifier 10.1109/TVT.2005.858172

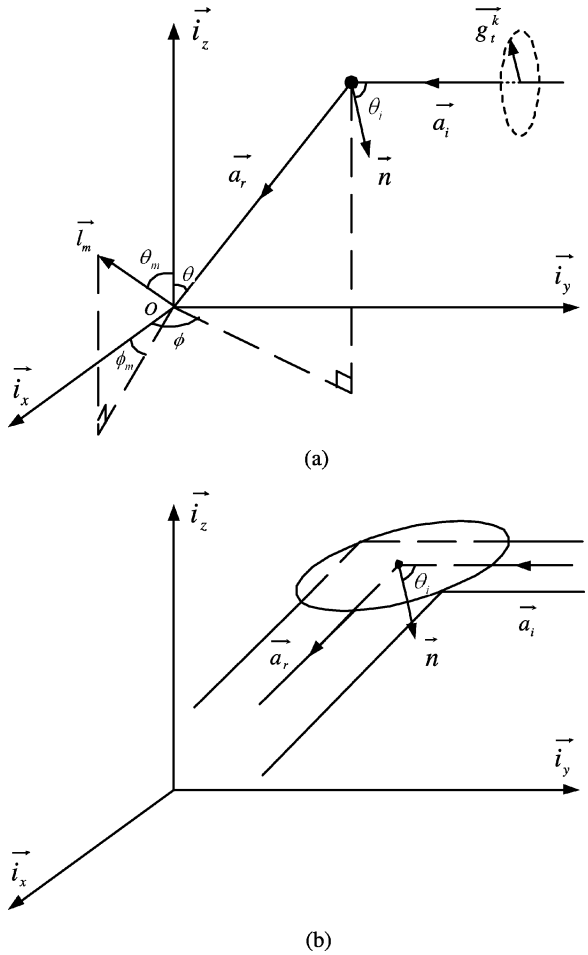

Fig. 1. System geometry.

II. System Model

Before the analysis, the assumptions on the channel model are briefly described as follows. 1) Assumptions about reflector distribution: the Model Station (MS) is surrounded by a large number of local reflectors uniformly distributed within the solid region defined in (15). Each reflector has uncorrelated amplitude, equal power, and the same dielectric constant k_ϵ. The sum of reflector powers is normalized to 1. 2) Assumptions about reflection: each wave received by the MS is only reflected by a single reflector. The reflector radius is much smaller than the MS-BS distance and, therefore, the waves from the BS are approximately parallel when reaching the reflectors.[1] Each reflector is further modeled as a properly oriented small plane so that the wave is redirected to the MS in the specular reflection direction.

A. Polarization Vector of Reflected Field

1) System Geometry: In this section, the effect of reflection on polarization will be examined. First, the MS is assumed to be located at the origin O of the rectangular coordinate system in Fig. 1(a), where $\vec{i}_x$, $\vec{i}_y$, and $\vec{i}_z$ represent the unit vectors corresponding to the three coordinate axes. Without loss of generality, the direction of the (BS) is assumed to be $\vec{i}_y$, as seen from the MS. Assuming the distance between the MS and the BS is much larger than the radius of the local reflectors around the MS, the propagation direction of each ray from the BS is approximately parallel to $-\vec{i}_y$ before reaching each reflector. In other words, the path angular spread is small at the BS. With the far-field assumption [2], [4], the reflector in Fig. 1(a) can be regarded as a point source in a distinct direction $\{\theta, \phi\}$, where θ and ϕ denote the elevation angle and azimuthal angle, respectively. It is also assumed that each signal received at the MS is a plane wave and has interacted with only a single reflector in the channel [15], [18], [22].

In order to study the polarization of the scattered wave, the scattering has to be modeled in a more detailed manner. Let $\vec{a}_i$ and $\vec{a}_r$ in Fig. 1(a) be the unit vectors for the directions of the incident and scattered waves, respectively, and another unit vector is defined as $\vec{n} = (\vec{a}_r - \vec{a}_i)/\parallel \vec{a}_r - \vec{a}_i \parallel$. It is natural to model the reflector, which is magnified in Fig. 1(b), as a small plane perpendicular to $\vec{n}$ so that the induced wave can just go along the specular reflection direction.[2] The polarization of the scattered wave can be determined by considering the reflection on this small plane. As shown in Fig. 1(b), the unit vectors for the directions of the incident and reflected plane waves are, respectively, given by

$$\vec{a}_i = -\vec{i}_y$$
$$\vec{a}_r = -(\cos\theta\,\vec{i}_z + \sin\theta\cos\phi\,\vec{i}_x + \sin\theta\sin\phi\,\vec{i}_y). \quad (1)$$

Accordingly, the incident angle θ_i is determined by $\cos\theta_i = \parallel \vec{a}_r - \vec{a}_i \parallel /2$ and the unit vector normal to the small reflection plane is $\vec{n} = (\vec{a}_r - \vec{a}_i)/(2\cos\theta_i)$.

2) Polarization Vector of Reflected Field: Suppose the incident wave from the transmitter travels in the negative y direction with linear polarization. The expression of the instantaneous incident field at an arbitrary point on the small plane in Fig. 1(b) is given by

$$\vec{E}_i = E_i\vec{g}_t = E_{ix}\vec{i}_x + E_{iz}\vec{i}_z \quad (2)$$

where the direction of the transmit polarization $\vec{g}_t$ is determined by the transmit antenna and is given by

$$\vec{g}_t = \eta_x\vec{i}_x + \sqrt{1-\eta_x^2}\,\vec{i}_z \quad (3)$$

which rotates from $\vec{i}_x$ to $\vec{i}_z$ as η_x varies from 1 to 0. The two field components in (2) now can be specified as $E_{ix} = E_i\eta_x$ and $E_{iz} = E_i\sqrt{1-\eta_x^2}$.

The reflected field is determined by the Fresnel reflection law [1, ch. 6, Eqn. 1.13] in (4), shown at the bottom of the next page, where "$\cdot$" and "$\times$" represent dot product and vector product, respectively. The reflection coefficients for the field components parallel and perpendicular to the incident plane are given by [1] and [7].

[1]Equivalently, the path angular spread at the BS is approximately zero.

[2]This is based on the idea from rough surface scattering that states that the polarization of the scattered field is the same as that of a field reflected from a plate oriented so that the specular reflection coincides with the scattering direction [27].

$$r_l = \frac{k_\epsilon \cos\theta_i - \sqrt{k_\epsilon - \sin^2\theta_i}}{k_\epsilon \cos\theta_i + \sqrt{k_\epsilon - \sin^2\theta_i}} = \frac{k_\epsilon\sqrt{1-\sin\theta\sin\phi} - \sqrt{2k_\epsilon - 1 - \sin\theta\sin\phi}}{k_\epsilon\sqrt{1-\sin\theta\sin\phi} + \sqrt{2k_\epsilon - 1 - \sin\theta\sin\phi}}$$

$$r_s = \frac{\cos\theta_i - \sqrt{k_\epsilon - \sin^2\theta_i}}{\cos\theta_i + \sqrt{k_\epsilon - \sin^2\theta_i}} = \frac{\sqrt{1-\sin\theta\sin\phi} - \sqrt{2k_\epsilon - 1 - \sin\theta\sin\phi}}{\sqrt{1-\sin\theta\sin\phi} + \sqrt{2k_\epsilon - 1 - \sin\theta\sin\phi}} \quad (5)$$

where k_ϵ denotes the dielectric constant.[3] After substituting the terms between (1) and (2) for their counterparts in (4) and following the steps in Appendix A, we can get the expression for the reflected field

$$\overrightarrow{E}_r = E_i(f_x \overrightarrow{i}_x + f_y \overrightarrow{i}_y + f_z \overrightarrow{i}_z) \triangleq E_i \overrightarrow{g}_r \quad (6)$$

where

$$f_x = \Big[r_s\left(\eta_x\cos^2\theta - \sqrt{1-\eta_x^2}\sin\theta\cos\theta\cos\phi\right) + r_l\left(\eta_x\sin^3\theta\cos^2\phi\sin\phi + \sqrt{1-\eta_x^2}\sin^2\theta\cos\theta\sin\phi\cos\phi\right)\Big] \Big/ (1-\sin^2\theta\sin^2\phi)$$

$$f_y = \Big[r_l\left(\eta_x\sin^3\theta\sin^2\phi\cos\phi + \sqrt{1-\eta_x^2}\sin^2\theta\cos\theta\sin^2\phi - \eta_x\sin\theta\cos\phi - \sqrt{1-\eta_x^2}\cos\theta\right)\Big] \Big/ (1-\sin^2\theta\sin^2\phi)$$

$$f_z = \Big[r_s\left(\sqrt{1-\eta_x^2}\sin^2\theta\cos^2\phi - \eta_x\sin\theta\cos\theta\cos\phi\right) + r_l\left(\eta_x\sin^2\theta\cos\theta\sin\phi\cos\phi + \sqrt{1-\eta_x^2}\sin\theta\cos^2\theta\sin\phi\right)\Big] \Big/ (1-\sin^2\theta\sin^2\phi). \quad (7)$$

The polarization vector $\overrightarrow{g}_r$ defined in (6) can be fully expanded by (7) and (5). It accounts for the changes of both polarization direction and amplitude of the field during the reflection process. Note that the norm of $\overrightarrow{g}_r$ is almost always less than one due to the reflection attenuation. Although the full expression of $\overrightarrow{g}_r$ is somewhat complicated, it relates the polarization vector with only four essential parameters, θ, ϕ, η_x, and k_ϵ.

B. Correlation of Multipolarization Antennas

1) Model of Received Signals: In this section, the expression of the received signal at the MS is derived when several colocated antennas with different polarizations are employed at both ends for diversity. Assuming binary-phase-shift-keying (BPSK) modulation, the baseband modulated symbol waveform is represented by $s(t)$ for $+1$ and $-s(t)$ for -1, where the pulse-shape waveform $s(t)$ is assumed to be constant during $[0, T]$ and 0 elsewhere. Without loss of generality, $+1$ is assumed to be sent by the BS. Moreover, there are K colocated transmit antennas with different polarizations at the BS and, as an example of transmit diversity signaling, a distinct orthogonal code $c_k(t)$ is assigned to the kth transmit antenna[4] so that the baseband signal on this antenna is $d_k(t) = s(t)c_k(t)$. Therefore, the signals on the K transmit signals are orthogonal to each other

$$\int_0^T d_k(t)d_{k'}(t)\,dt = \frac{E_b}{K}\delta_{kk'} \quad (8)$$

where T represents the symbol duration, and E_b/K is the energy of $d_k(t)$. The total energy of the K transmit signals is E_b and is always constant. Moreover, $d_k(t)$ is assumed to be narrowband.

It is assumed that there are N local reflectors around the MS, which is located at the origin O in Fig. 1(a). The reflector number is large and they are uniformly distributed within the solid region defined in (15). Without loss of generality, the reflector in Fig. 1(a) represents the nth reflector. The wave introduced by the kth transmit antenna reaches the nth reflector in the direction $\overrightarrow{a}_i$ with transmit polarization direction $\overrightarrow{g}_t^k$, which is determined by η_x^k in (3). After the reflection, the reflected wave reaches the MS with the field

$$\overrightarrow{E}_n^k(t) = d_k(t-\tau_n)\alpha_n \overrightarrow{g}_{rn}^k \quad (9)$$

where r_n is the corresponding propagation delay, α_n represents the amplitude decay and phase shift caused by the distance, and the polarization vector of the reflected field $\overrightarrow{g}_{rn}^k$ is specified in (6). Supposing the MS antenna array consists of M colocated dipole antennas with different orientations, the unit vector for the orientation of the mth receive antenna is illustrated in Fig.1(a) and is given by

$$\overrightarrow{l}_m = \sin\theta_m\cos\phi_m \overrightarrow{i}_x + \sin\theta_m\sin\phi_m \overrightarrow{i}_y + \cos\theta_m \overrightarrow{i}_z \quad (10)$$

which is a function of θ_m and ϕ_m. According to [3], [6], and [9], the received signal voltage induced by $\overrightarrow{E}_n^k(t)$ is proportional to

$$u_{nm}^k(t) = \overrightarrow{E}_n^k(t) \cdot \overrightarrow{l}_m \quad (11)$$

and the total signal brought by the kth transmit antenna is the sum of signals from all N reflectors $\sum_{n=1}^N u_{nm}^k(t)$. The signal on the mth receive antenna comprises the contributions from all K transmit antennas plus the background noise

$$r_m(t) = \sum_{k=1}^K\sum_{n=1}^N u_{nm}^k(t) + w_m(t) = \sum_{k=1}^K d_k(t-\tau)\sum_{n=1}^N \alpha_n(\overrightarrow{g}_{rn}^k \cdot \overrightarrow{l}_m) + w_m(t) \quad (12)$$

[3]Typical values of dielectirc constants of some prominent dielectric materials are tabulated in [7].

[4]This method is named orthogonal TD-simulcast in [21].

$$\overrightarrow{E}_r = \frac{r_s[\overrightarrow{n}\cdot(\overrightarrow{a}_i \times \overrightarrow{E}_i)](\overrightarrow{n}\times\overrightarrow{a}_i) - r_l(\overrightarrow{n}\cdot\overrightarrow{E}_i)(\cos\theta_i\overrightarrow{a}_i + \cos2\theta_i\overrightarrow{n})}{\sin^2\theta_i} \quad (4)$$

where all paths are assumed to have the same delay τ due to the narrowband assumption. The matched filter output at the mth receive antenna corresponding to the kth transmit antenna can be then written as

$$\begin{aligned} U_m^k &= \int_\tau^{T+\tau} r_m(t) d_k(t-\tau)\, dt \\ &= \frac{E_b}{K} \sum_{n=1}^{N} \alpha_n (\overrightarrow{g}_{rn}^k \cdot \overrightarrow{l}_m) \\ &\quad + \int_\tau^{T+\tau} w_m(t) d_k(t-\tau)\, dt \triangleq \frac{E_b}{K} H_m^k + N_m^k \end{aligned} \quad (13)$$

where H_m^k denotes the channel coefficient associated with the mth receive and kth transmit antennas.

2) Correlation of Channel Coefficients: It is assumed that the reflector amplitude α_n is uncorrelated with equal power: $E[\alpha_n \alpha_{n'}^*] = \delta_{nn'}/N$. The correlation between the channel coefficients associated with different tranmit-receive antenna pairs is given by

$$\begin{aligned} &R_H(m, m', k, k') \\ &\quad = E\left[H_m^k H_{m'}^{k'*}\right] \\ &\quad = \sum_{n=1}^{N} \frac{1}{N} \left[\overrightarrow{g}_r^k(\theta_n, \phi_n) \cdot \overrightarrow{l}_m\right] \left[\overrightarrow{g}_r^{k'}(\theta_n, \phi_n) \cdot \overrightarrow{l}_{m'}\right] \\ &\quad \triangleq \sum_{n=1}^{N} \frac{1}{N} f(\theta_n, \phi_n) \end{aligned} \quad (14)$$

where $\overrightarrow{g}_r^k(\theta_n, \phi_n)$ is used instead of $\overrightarrow{g}_{rn}^k$ to emphasize that it is a function of the reflector direction. The reflector number N is large, and they are assumed to be uniformly distributed within a solid region

$$\begin{aligned} \Omega(\upsilon, \beta) = \Big\{ (\theta, \phi) \;\Big|\; &\theta \in \left[\frac{\pi}{2} - \upsilon, \frac{\pi}{2} - \beta\right] \\ &\text{with} -\frac{\pi}{2} \le \beta < \upsilon \le \frac{\pi}{2}, \quad \phi \in [0, 2\pi) \Big\}. \end{aligned} \quad (15)$$

The solid angle of this region is $A_\Omega = \iint_{\Omega(\upsilon,\beta)} d\Omega = 2\pi(\sin\upsilon - \sin\beta)$. As N approaches infinity, the reflector number in $d\Omega$ at (θ, ϕ) is $(N/A_\Omega)d\Omega$, and their contributions to $R_H(m, m', k, k')$ are $(f(\theta, \phi)/A_\Omega)d\Omega$. Therefore, as $N \to \infty$, (14) can be written as

$$\begin{aligned} &R_H(m, m', k, k') \\ &\quad = \iint_{\Omega(\upsilon,\beta)} f(\theta, \phi) \frac{1}{A_\Omega} d\Omega \\ &\quad = \int_0^{2\pi} \int_{\frac{\pi}{2}-\upsilon}^{\frac{\pi}{2}-\beta} \left[\overrightarrow{g}_r^k(\theta, \phi) \cdot \overrightarrow{l}_m\right] \\ &\qquad \times \left[\overrightarrow{g}_r^{k'}(\theta, \phi) \cdot \overrightarrow{l}_{m'}\right] \frac{1}{2\pi(\sin\upsilon - \sin\beta)} \sin\theta\, d\theta\, d\phi \end{aligned} \quad (16)$$

where $\overrightarrow{l}_m$ is given by (10), and $\overrightarrow{g}_r^k$ is defined in (6). It is clear that the correlation is a function of the elevation of reflectors $[\beta, \upsilon]$, the receive antenna orientations $\{\overrightarrow{l}_m, \overrightarrow{l}_{m'}\}$, the transmit antenna polarizations $\{\eta_x^k, \eta_x^{k'}\}$, and the dielectric constant k_ϵ. Recall that $\overrightarrow{g}_r^k$ is also a function of η_x^k and k_ϵ. Here, all reflectors are assumed to have the same k_ϵ to simplify the analysis. The channel power $E[|H_m^k|^2]$ can be obtained by setting $k' = k$ and $m' = m$ in (16).

The effectiveness of a polarization diversity system is often assessed by cross polarization discrimination (XPD), which is equal to the ratio of channel powers associated with two orthogonal receive antennas in the (17), shown at the bottom of the page.

3) Probability of Error and Channel Capacity: The probability of error is used to evaluate the performance of the polarization diversity system. It is assumed that the complex Gaussian noise $w_m(t)$ in N_m^k defined in (13) is white with power spectrum density $N_0 : E[w_m(t) w_m^*(t')] = N_0\, \delta(t - t')$, and hence, we have

$$\begin{aligned} E\left[|N_m^k|^2\right] &= E\left\{ \int_\tau^{T+\tau} w_m(t) d_k(t-\tau)\, dt \right. \\ &\qquad \left. \times \int_\tau^{T+\tau} w_m^*(t') d_k(t'-\tau)\, dt' \right\} \\ &= N_0 \int_\tau^{T+\tau} d_k^2(t-\tau)\, dt = N_0 \frac{E_b}{K}. \end{aligned} \quad (18)$$

Consequently, the average signal to noise ratio (SNR) at the matched filter output at the mth receive antenna corresponding to the kth transmit antenna is

$$\bar{\gamma}_m^k = \frac{E_b^2 E\left[|H_m^k|^2\right]}{K^2 E\left[|N_m^k|^2\right]} = \frac{E_b E\left[|H_m^k|^2\right]}{K N_0}. \quad (19)$$

In addition, the $KM \times 1$ channel coefficient vector is defined as $\boldsymbol{h} = [\boldsymbol{h}_1, \ldots, \boldsymbol{h}_K]^T$ with $\boldsymbol{h}_k = [H_1^k, \ldots, H_M^k]$, and the corresponding $KM \times KM$ channel correlation matrix is $\mathbf{R} = E[\boldsymbol{h}\boldsymbol{h}^H]$. Eigendecomposition is further performed on the correlation matrix: $\mathbf{\Lambda} = \mathbf{Q}^H \mathbf{R} \mathbf{Q}$, where $\mathbf{Q}$ denotes the complete set of orthonormal eigenvectors of $\mathbf{R}$. According to [32], the power for each equivalent independent channel is represented by λ_j, which is the jth diagonal element of $\mathbf{\Lambda}$, and the corresponding transformed branch SNR is given by

$$\bar{\gamma}_j = \frac{E_b \lambda_j}{K N_0}, \quad j = 1, \ldots, KM. \quad (20)$$

$$\text{XPD} = \begin{cases} \dfrac{E\left[|H_m^k|^2\right] \text{ with } \eta_x^k = 0 \text{ and } \overrightarrow{l}_m = \overrightarrow{i}_z}{E\left[|H_m^k|^2\right] \text{ with } \eta_x^k = 0 \text{ and } \overrightarrow{l}_m = \overrightarrow{i}_x}, & \text{for vertical transmit polarization} \\ \dfrac{E\left[|H_m^k|^2\right] \text{ with } \eta_x^k = 1 \text{ and } \overrightarrow{l}_m = \overrightarrow{i}_x}{E\left[|H_m^k|^2\right] \text{ with } \eta_x^k = 1 \text{ and } \overrightarrow{l}_m = \overrightarrow{i}_z}, & \text{for horizontal transmit polarization.} \end{cases} \quad (17)$$

The optimal symbol decision is obtained by combining the KM matched filter outputs with a maximum ratio combiner, and the corresponding probability of error is given by [12]

$$P_e = \frac{1}{2}\sum_{j=1}^{KM}\pi_j\left[1-\sqrt{\frac{\overline{\gamma}_j}{1+\overline{\gamma}_j}}\right], \text{where } \pi_j = \prod_{\substack{i=1\\ i\neq j}}^{KM}\frac{\overline{\gamma}_j}{\overline{\gamma}_j-\overline{\gamma}_i}. \tag{21}$$

On the other hand, for a $M \times K$ MIMO system, the ergodic channel capacity with uniform power allocation is given by [17], [20], [23]

$$C = E\left[\log_2 \det\left(\mathbf{I}_M + \frac{\rho}{K}\mathbf{H}\mathbf{H}^H\right)\right] \text{ bps/Hz} \tag{22}$$

where $\mathbf{H} = [\boldsymbol{h}_1^T, \ldots, \boldsymbol{h}_K^T]$ denotes the $M \times K$ channel transfer matrix, $\rho = E_b/N_0$ is the total transmit SNR, $\mathbf{I}_M$ represents the $M \times M$ identity matrix, and the expectation is over different realizations of $\mathbf{H}$.

III. Numerical Results

A. Channel Depolarization

This section investigates the depolarization effect caused by a channel with a large number of reflectors uniformly distributed within the solid region in (15). In most experiments, the channel depolarization is measured by XPD, which reflects the decoupling of signal energy into the orthogonal polarizations. The XPD was evaluated according to (17) and is plotted in Fig. 2(a) for vertical transmit polarization. Since the MS is usually close to the ground, most reflectors are higher than the MS and, therefore, β in (15) is chosen to be 0° in all subsequent results. The impact of different β values on the performance will be discussed in Section III-B. Moreover, four k_ϵ values from 2 to 16 are considered, and this range includes most solid materials. It is apparent that XPD decreases with the increase of υ, which represents the range of the reflector elevation angle θ. The reduction of XPD is about 9 dB when υ changes from 15° to 75° for each k_ϵ. When υ is small, each incoming wave contains a large proportion of vertical polarization and, hence, the corresponding XPD is high. However, more oblique incoming waves with abundant horizontal components will be included when υ increases, and that leads to the decrease of XPD. Overall, the reduction of XPD is less than 4 dB when k_ϵ increases from 2 to 16 for each fixed υ.

It is also necessary to compare the analysis with measured values. In [8], XPD measurement was conducted in outdoor mobile radio environments. Vertical polarization was used for transmission, and half-wave dipole antennas were employed at the MS as the vertical and horizontal reference antennas. The measured XPD is about 4–7 dB in urban areas and is more than 11 dB in rural areas. The variation trend of XPD in the measurements is basically consistent with that in Fig. 2(a), in which XPD decreases for larger υ which could represent the change from the rural area to the urban area. In addition, the measured XPD in most uplink experiments [3], [6], [9] is about 6–7 dB in urban areas and is around 12 dB in rural areas. It is also reported in [6] that XPD is larger for high-low mixed building areas and is lower for high-building-concentrated areas. The variation trend of XPD in these experimental results basically agrees with the analysis.

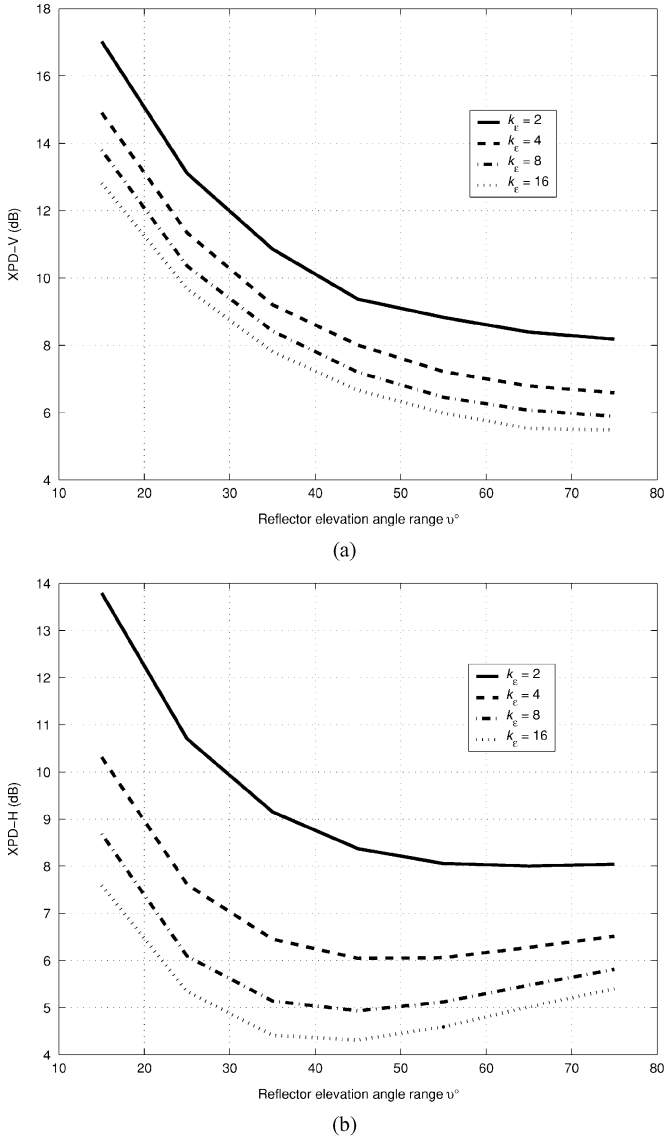

Fig. 2. Cross polarization discrimination. (a) Vertical transmit polarization. (b) Horizontal transmit polarization.

The results for horizontal transmit polarization are plotted in Fig. 2(b). Compared with that in Fig. 2(a), XPD varies less significantly with υ. In addition, most values are confined to the range of 4–10 dB and are less than those in vertical case, especially when υ is small. For both transmit polarizations, the XPD decreases in general for larger υ, which implies that the effect of channel depolarization becomes more significant as υ increases.

B. Error Probability for Different Antenna Configurations

In the downlink communication from the BS to the MS, the MS is located at the origin O in Fig. 1(a), while the BS is in the direction $\overrightarrow{i}_y$. Both MS and BS are equipped with

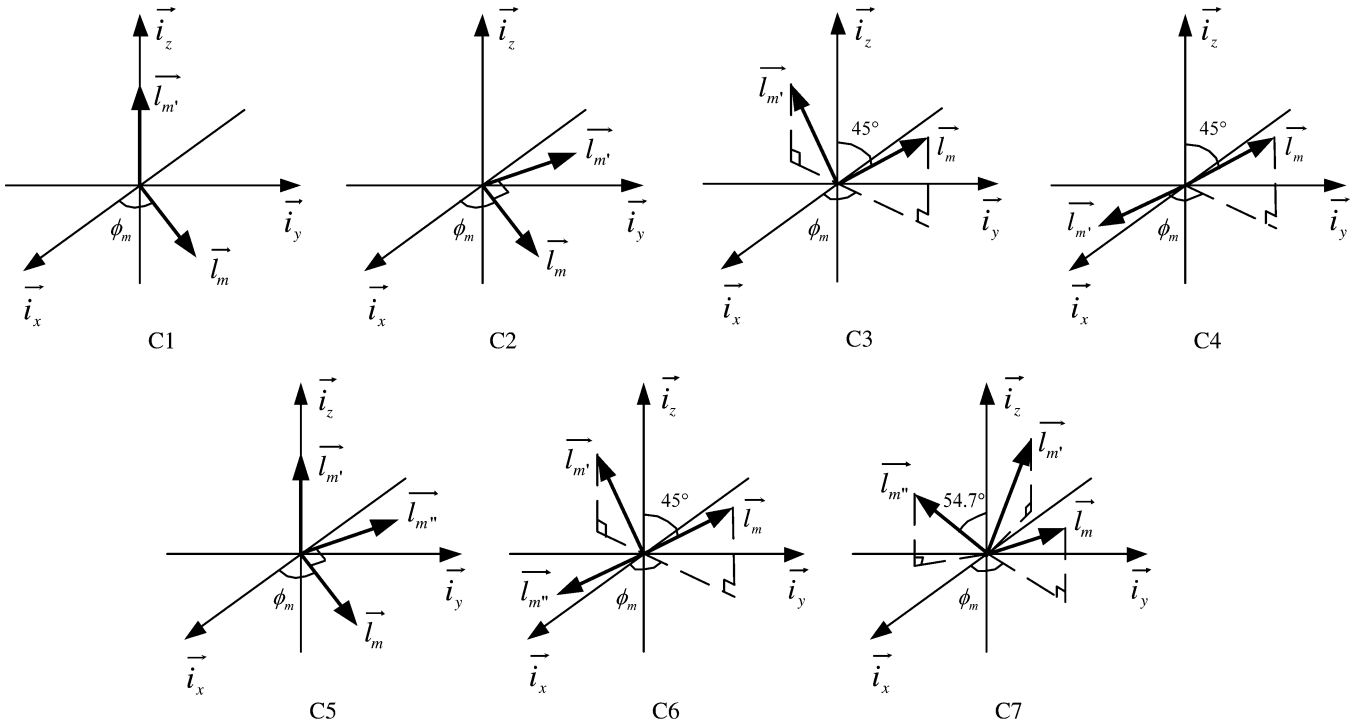

Fig. 3. Multipolarization antenna configurations at the MS.

a certain number of colocated multipolarization transmit and receive antennas. Several possible multipolarization antenna configurations at the MS are illustrated in Fig. 3 and are denoted by C1–C7. C1–C4 contain two orthogonal antenna branches, whose polarizations are vertical/ horizontal, double horizontal, double 45° slanted, and 45° slanted/horizontal, respectively. C5–C7 have three orthogonal branches, whose polarizations are vertical/double horizontal, double 45° slanted/horizontal, and triple 54.7° slanted, respectively. The horizontal orientation angle ϕ_m of the branch m is marked to identify the rotations of the configuration in the horizontal plane. In the following results, k_ϵ is fixed as 8, which is typical for construction materials.

A single transmit antenna is first considered at the BS. For each MS configuration, the error probability P_e is computed using (21) for fixed ϕ_m and υ, and E_b/N_0 is chosen to be 30 dB. The P_e at each υ is further averaged over 36 different ϕ_m with 10° apart[5] and is plotted in Fig. 4(a) for vertical transmit polarization, which is in the direction $\vec{i}_z$ in Fig. 1(a). As a reference, a single vertical (SV) receive antenna is also included in the comparison. It is obvious that the P_e of SV is large due to the lack of diversity. As for the two-antenna configurations C1–C4, C2 always gives the larger P_e, which is even higher than that of SV when υ is less than 25°. This is because both antennas in C2 receive horizontal polarization, which is relatively scarce especially when υ is small. However, as implied in Fig. 2(a), the horizontal component becomes increasingly abundant with the increase of υ, and that leads to the decrease in P_e. Meanwhile, both C1 and C3 achieve the smaller P_e of the four. As for the three-antenna configurations C5–C7, great P_e improvements are achieved by all of them, and they also have the same performance. As shown in Appendix B, the error probability[6] is indeed invariant to the orientations of the three-branch orthogonal structure, since the three-dimensional signal space is spanned by three mutually orthogonal vectors with any orientation. Numerical investigation also indicates that adding the fourth or more receive antennas only yields a slight P_e improvement, which is caused not by diversity but by capturing more power. Finally, it can be observed in Fig. 4(a) that P_e gets smaller for C1–C7 as υ increases due to the reduction of XPD.

The P_e performance in case of one transmit antenna with horizontal polarization is presented in Fig. 4(b). In contrast to Fig. 4(a), the performance varies less significantly with υ for all MS configurations, since the XPD for horizontal transmit polarization is less sensitive to υ. Without diversity, the P_e of a single horizontal (SH) antenna is naturally above those of other configurations. Among all twoantenna configurations, C2 achieves the best performance, since horizontal polarization is used for transmission. Both C1 and C3 result in the same P_e, and the performance of C4 is in between. As for the three-antenna configurations, identical performance is again observed for all of them.

In the following, the diversity performance is investigated for more than one transmit antenna. Two colocated antennas are first considered at the BS with vertical and horizontal (V/H) polarizations. The polarization directions are $\vec{i}_z$ and $\vec{i}_x$, respectively, when their signals reach the reflector in Fig. 1(a). The

[5]Since the MS configuration may rotate in the horizontal plane due to the mobile movement, P_e is evaluated at different rotation angle ϕ_m in Fig. 3 and is further averaged to remove the impact of receiver rotations on the error probability. However, the rotation will not affect the P_e for C5–C7, as explained later.

[6]This is determined by the eigenvalues of channel correlation matrix.

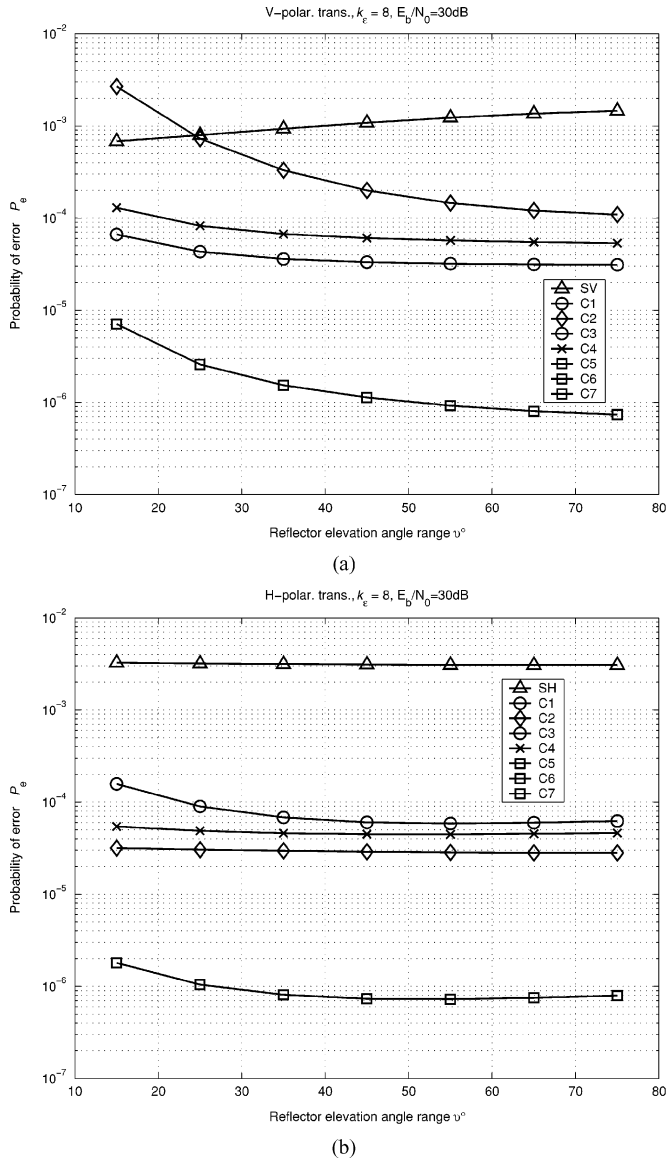

Fig. 4. Probability of error for different MS antenna configurations in case of one transmit antenna. (a) Vertical transmit polarization. (b) Horizontal transmit polarization.

results are presented in Fig. 5, in which E_b represents the total transmitted signal energy. Compared with Fig. 4, the error probability has decreased by about one or two orders of magnitude for all MS configurations. Among two-antenna configurations, C4 achieves the lowest error probability. The improvement is again significantly boosted by all three-antenna MS configurations C5–C7, which have the same performance as observed before.

Besides the V/H configuration, we are also interested in the error probability when the two transmit antennas are rotated to other directions. The P_e is calculated for the $\pm 45^\circ$ configuration formed by rotating the V/H configuration by 45°. It is observed that the error probability curves are exactly the same as those in Fig. 5. The same performance is because the eigenvalues of $\mathbf{R}$ are independent of the rotations, as shown in Appendix C. This also coincides with the intuition that two orthogonal vectors at any rotation angle span the same two-dimensional signal space.

We now summarize the results for the rank of $\mathbf{R}$, which primarily determines the diversity performance. For one transmit antenna, the rank is the same as the number of orthogonal receive antennas and is limited to three. In case of two orthogonal transmit antennas and three orthogonal receive antennas, the rank of the 6×6 channel correlation matrix will be six corresponding to the same number of independent diversity branches. If the above polarization configurations are incorporated into spatial diversity, the number of diversity branches will be increased by a factor of six for the same space, and hence, a great performance improvement can be expected.

However, since the path angular spread is assumed to be approximately zero at the BS, only two orthogonal transmit antennas perpendicular to the direction of the MS are considered. This is because if the third orthogonal antenna is used, it will be parallel to the MS direction and cannot transmit signal in that direction. As pointed out in [31], for large angular spread, the third transmit polarization can be utilized as well, since the signal transmitted by the third antenna can reach the MS via the paths not in the MS direction. In this case, the optimum BS configuration would be the one exploiting all three orthogonal transmit polarizations.

Another interesting observation is that almost in all cases, the error probability goes down with the increase of υ, which controls the reflector elevation, e.g., large υ corresponds to high-building-concentrated areas. Therefore, one can infer that polarization diversity will have better performance in urban areas with densely located highrise buildings than in rural areas with lowrise structures. In addition, it is also instructive to study the P_e for β greater than zero.[7] To do this, the P_e in Fig. 5 is recomputed by setting $\upsilon = 75^\circ$ while varying β from 0° to 60°. It is interesting to note that the P_e increases with β for all configurations, while the relation between them remains the same. This result essentially coincides with Fig. 5 and again confirms the fact that smaller distribution range of reflectors will generally cause higher P_e due to the decreased channel depolarization effect. This observation is similar to the relation between scattering and spatial correlation [23]: The spatial correlation increases as the reflector angular spread decreases, and that causes performance degradation.

The impact of SNR on diversity performance has also been studied, and five combinations with different diversity orders[8] are selected for comparison. In Fig. 6, V-SV refers to the case when a single vertically polarized antenna is used at each end, V-C1 represents the combination of C1 and one vertically polarized transmit antenna, and VH-C1 includes the second transmit antenna with horizontal polarization. From V-SV to VH-C5 in the figure, the diversity order increases from one to six. Apparently, for each combination, P_e decreases for higher SNR. At a given SNR, P_e decreases from V-SV to VH-C5 due to the increased diversity order. In addition, the P_e

[7]Note that β is chosen to be 0° in the previous results.

[8]This is equal to the rank of channel correlation matrix.

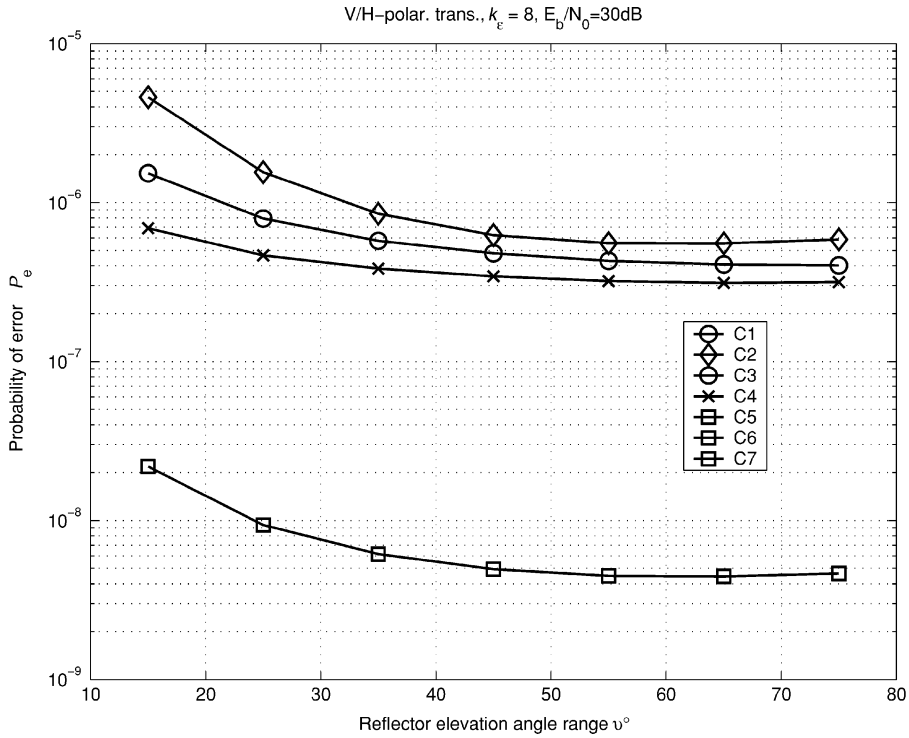

Fig. 5. Probability of error for different MS antenna configurations in case of two transmit antennas with vertical/horizontal polarizations.

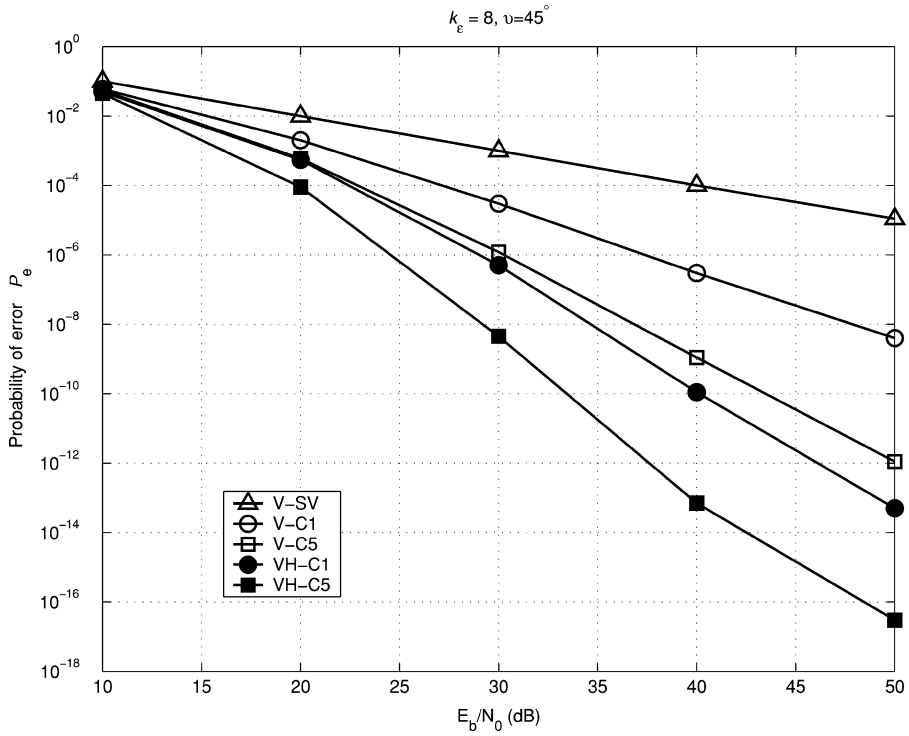

Fig. 6. Probability of error for different SNR.

reduction due to higher diversity order is more evident at higher SNR.

To realize polarization diversity, implementation issues need to be considered at both sides, especially at the MS due to the space constraints. One implementation example can be found in [30]. At the MS, a dual polarized array with 45° slanted monopole elements is mounted on the top of a laptop, while at the BS, a dual polarized array with 45° slanted elements is oriented toward the served sector. In [34], the polarization diversity is realized by two orthogonal branches of a

cross-shaped patch antenna which could be mounted on the surface of a handset. It is also possible to exploit the third polarization by installing a monopole orthogonal to that surface. Another design for small terminals can be found in [16], in which two orthogonal elements are located at one side of a wireless IC card.

C. Channel Capacity for Different Antenna Configurations

The channel capacity is first studied in case of one transmit antenna. For each MS configuration, the channel correlation matrix matrix $\mathbf{R}$ is computed via (16) for fixed ϕ_m and υ. Using this correlation matrix, 10^3 channel vector realizations are generated according to $\boldsymbol{h} = \mathbf{R}^{1/2}\boldsymbol{w}$, where $\boldsymbol{w}$ is a $KM \times 1$ complex Gaussian random vector with zero mean and unit variance. Next, each $\boldsymbol{h}$ is reshaped to the $M \times K$ channel matrix $\mathbf{H}$, and the corresponding ergodic capacity is computed using (22). The transmit SNR ρ is 30 dB in the evaluation. The capacity is further averaged over 36 different ϕ_m with 10° apart and is plotted against υ in Fig. 7(a) for vertical transmit polarization. It can be observed that the capacity improves from C2 to C7. This improvement is due to the increase of received signal energy. Since both antennas in C2 receive horizontal polarization, it always gives the lowest capacity, which is even lower than that of SV. However, the capacity of C2 increases for larger υ, since more signal energy is decoupled into the horizontal polarization, but that also results in the capacity reduction of SV. The three-antenna configurations C5–C7 again achieve the same capacity,[9] but compared with the great P_e improvement in Fig. 4(a), the capacity improvement over twoantenna configurations is not significant. For instance, the capacity improvement of C5 over C1 is always less than 3.2%. This is due to the fact that in diversity, the improvement is mainly determined by the rank of $\mathbf{R}$, while for capacity, the improvement is mainly controlled by the number of parallel channels, which is the rank of $\mathbf{H}\mathbf{H}^H$. For one transmit antenna, only one parallel channel exists, and more receive antennas result in higher channel SNR, which only improves the channel capacity logrithmicaly.

Fig. 7(b) shows the channel capacity in case of one transmit antenna with horizontal polarization. The capacity improvement from SH to C7 is again due to the increase of received signal energy. Because the horizontal polarization is used for transmission, C4 achieves the highest capacity among all two antenna configurations, but the improvement over SH is still insignificant.

The capacity performance for two transmit antennas with V/H polarizations is presented in Fig. 8, and like the case in diversity, the capacity is invariant to the configuration rotations. The capacity improvement brought by the second transmit antenna is significant, and the improvement is more than 70% for almost all MS configurations over their counterparts in Fig. 7. This is because the rank of $\mathbf{H}\mathbf{H}^H$ now is two. In addition, the ratio of the two nonzero eigenvalues of $\mathbf{H}\mathbf{H}^H$ on average is between four to eight for most MS configurations when $\upsilon = 15^\circ$, and the ratio decreases to about 1 as υ increases to 75°.

[9]The slight difference is due to the finite number of realizations.

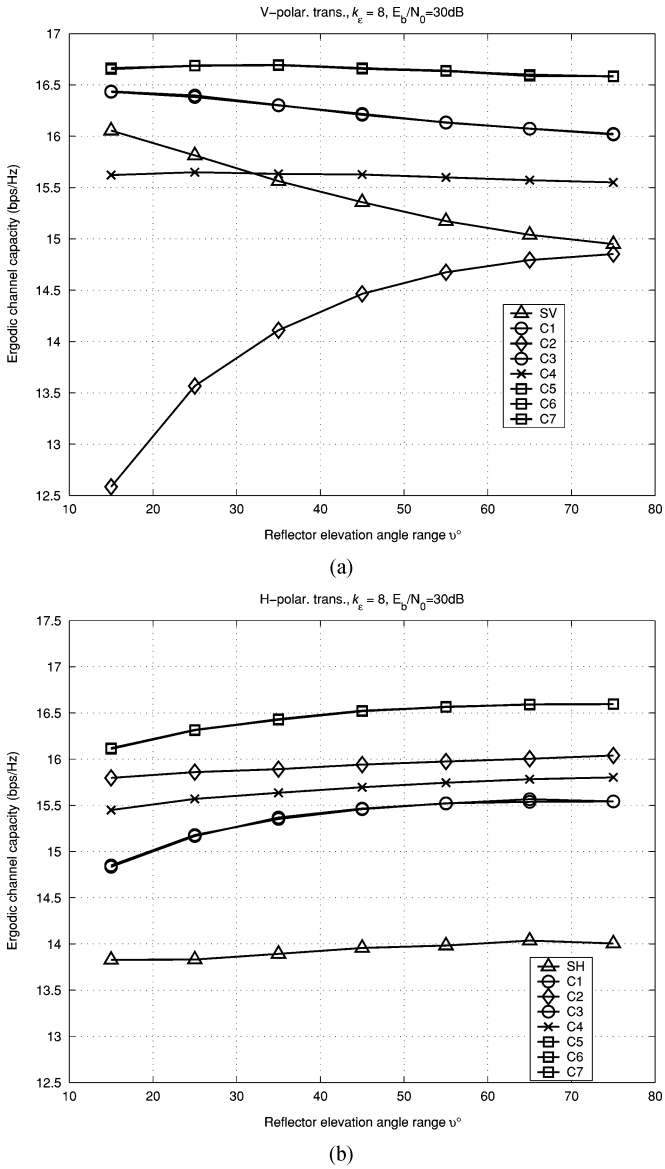

Fig. 7. Ergodic channel capacity for different MS antenna configurations in case of one transmit antenna. (a) Vertical transmit polarization. (b) Horizontal transmit polarization.

Based on above results, one can observe that most capacity gain is achieved by both C1 and C3 in conjunction with two transmit antennas in Fig. 8. The improvement brought by the third receive antennas is only about 10%. However, since the angular spread is assumed to be small at the BS, only two orthogonal transmit antennas perpendicular to the MS direction are considered. In the presence of large angular spread, all three transmit polarizations could be utilized to create three parallel channels, and the optimum configuration in this case would be the one with three orthogonal antennas at both sides. In addition, from Figs. 7(a) and 8, it is interesting to note that the capacity of C2 increases significantly with υ whenever vertical transmit polarization is used. The capacity improvement for larger υ is because more signal energy is captured by both horizontal antennas due to the increased leakage from vertical

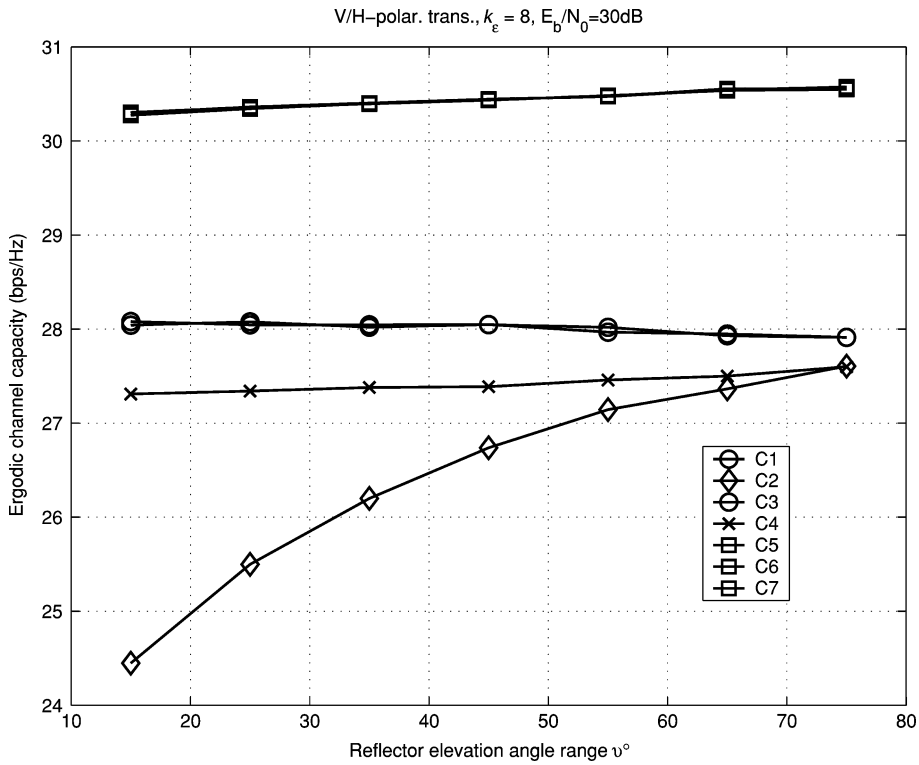

Fig. 8. Ergodic channel capacity for different MS antenna configurations in case of two transmit antennas with vertical/horizontal polarizations.

component to horizontal component. It would be instructive to compare the results with existing work. In [37], channel capacity is simulated for a configuration with three uncorrelated transmit antennas and three receive monopoles forming a structure like C7. The reflector elevation υ is chosen to be 30° for outdoor urban environment and 90° for indoor environment. It is found that the former almost achieves the same capacity as the latter. This is basically consistent with Fig. 8 in which the capacity of C7 only slightly increases with υ.

IV. Relation to Existing Work

Recently, a channel model for polarization diversity was proposed in [33], which compared polarization diversity with spatial diversity, and the channel conditions where the use of polarization diversity is beneficial were identified from the viewpoint of error probability. In [33], two $\pm 45^\circ$ slanted antennas are assumed at both ends, and the corresponding 2×2 MIMO channel transfer matrix comprises two parts: the fixed component $\tilde{\mathbf{H}}$; e.g., line-of-sight component, and the scattered component $\tilde{\mathbf{H}}$, which is also the emphasis of our work. The 4×4 channel correlation matrix $\mathbf{C}_{\tilde{y}}$ corresponding to $\tilde{\mathbf{H}}$ is modeled by (10) in [33]. For the particular $\pm 45^\circ$ slanted antenna configuration, the entries of $\mathbf{C}_{\tilde{y}}$ are symmetric and can be fully described by three parameters: the receive correlation r, the transmit correlation t, and α, which is related to the XPD. Although the symmetric pattern in $\mathbf{C}_{\tilde{y}}$ is appealing to analysis, it usually does not hold for other antenna polarization configurations, and thus, the analysis may not be applicable to other configurations, especially when the antenna configuration is not 2×2. Moreover, the relation between correlation and some physical channel characteristics, e.g., the reflector distribution, is not clear.

In our analysis, the channel correlation is studied theoretically based on the proposed model. An explicit expression (16) is derived for each entry in the channel correlation matrix. The correlation is described as a function of the antenna polarization configurations and the reflector distribution. Therefore, it is applicable to various antenna configurations, and the impact of the reflector distribution on performance can be assessed as well.

V. Conclusion

In this paper, a theoretical channel model has been proposed to study the performance of multipolarization antenna systems for downlink mobile communications. This model attempts to connect electromagnetics with communication theory and, based on this connection, the probability of error and channel capacity are studied numerically for different antenna configurations and scattering environments. The results enable us to predict the performance relationship between different configurations in realistic communication systems.

To simplify the analysis, a small path angular spread is assumed at the BS, while the MS is located in a rich scattering environment. As for the probability of error, considerable improvement can be achieved by increasing the number of orthogonal receive antennas from one to three at the MS. Furthermore, the error probability of the threebranch orthogonal structure is independent of its orientations, and the improvement is in significant for more receive antennas. At the BS, the

performance is greatly enhanced by using two transmit antennas that produce orthogonal polarizations in the direction of the MS, and the error probability is independent of rotations of the two transmit antennas. In case of three orthogonal receive antennas and two orthogonal transmit antennas, the 3×2 MIMO system results in a diversity order of six. As for the channel capacity, most capacity gain is achieved by the receive configuration C1 and C3 in conjunction with two orthogonal transmit antennas. The corresponding 2×2 MIMO system provides two parallel channels between the MS and the BS. Note that since the angular spread is small at the BS, only two orthogonal transmit antennas perpendicular to the MS direction are considered, and hence, the number of parallel channels is limited to two. It is also noteworthy that larger υ yields better performance in general. Therefore, multipolarization antenna systems would be more beneficial in areas with high rise structures.

In the presence of a large angular spread at the BS, the third orthogonal transmit polarization could be exploited as well, and the optimum configuration in this case would be the one with three orthogonal antennas at both sides. The corresponding 3×3 MIMO system will afford a diversity order of nine and three parallel channels, which further improve probability of error and channel capacity. In our future work, the analysis will be extended to array configurations incorporating both polarization diversity and spatial diversity, and the analytical results will be compared with other simulation techniques, such as the method of moments (MOMs) and the finit-difference timedomain (FDTD) techniques. Another important issue is the mutual coupling between antennas with different polarizations. Recent investigations [35], [36] show that mutual coupling can generally increase channel capacity. Therefore, it would be instructive to incorporate mutual coupling into the channel modeling and evaluate its impact on performance in our future work.

APPENDIX I
EXPRESSION OF THE REFLECTED FIELD

The scenario for the problem is depicted in Fig. 1, where $\overrightarrow{a}_i$, $\overrightarrow{a}_r$, θ_i, and $\overrightarrow{n}$ are specified in (Section II-A1). The purpose is to find the reflected field through (4) for an incident field at a point on the small plane in Fig. 1(b): $\overrightarrow{E}_i = E_{ix}\overrightarrow{i}_x + E_{iz}\overrightarrow{i}_z$. First of all, individual terms in (4) can be specified as (23), shown at the bottom of the page. Based on (23), the two terms in the numerator of (4) can be separately written as (23). The final expression of the reflected field (25) can be achieved by inserting (24) into (4). Both (24) and (25) are shown at the bottom of the next page. It can be easily shown that $\overrightarrow{E}_r \cdot \overrightarrow{a}_r = 0$, and thus, the derivation can be partially verified. The reflected field can be further rewritten as (6) by using the relations $E_{ix} = E_i\eta_x$ and $E_{iz} = E_i\sqrt{1-\eta_x^2}$.

$$
\begin{aligned}
&\cos\theta_i \overrightarrow{a}_i \\
&\quad = -\sqrt{\frac{1-\sin\theta\sin\phi}{2}}\overrightarrow{i}_y \\
&\cos 2\theta_i \overrightarrow{n} \\
&\quad = \frac{\sin\theta\sin\phi\cos\theta\overrightarrow{i}_z + \sin^2\theta\sin\phi\cos\phi\overrightarrow{i}_x - \sin\theta\sin\phi(1-\sin\theta\sin\phi)\overrightarrow{i}_y}{\sqrt{2(1-\sin\theta\sin\phi)}} \\
&\cos\theta_i \overrightarrow{a}_i + \cos 2\theta_i \overrightarrow{n} \\
&\quad = \frac{\sin\theta\sin\phi\cos\theta\overrightarrow{i}_z + \sin^2\theta\sin\phi\cos\phi\overrightarrow{i}_x + (\sin^2\theta\sin^2\phi - 1)\overrightarrow{i}_y}{\sqrt{2(1-\sin\theta\sin\phi)}} \\
&\overrightarrow{n} \times \overrightarrow{a}_i \\
&\quad = \frac{-\cos\theta\overrightarrow{i}_x + \sin\theta\cos\phi\overrightarrow{i}_z}{\sqrt{2(1-\sin\theta\sin\phi)}} \\
&\overrightarrow{a}_i \times \overrightarrow{E}_i \\
&\quad = E_{ix}\overrightarrow{i}_z - E_{iz}\overrightarrow{i}_x \\
&\overrightarrow{n} \cdot (\overrightarrow{a}_i \times \overrightarrow{E}_i) \\
&\quad = \frac{E_{iz}\sin\theta\cos\phi - E_{ix}\cos\theta}{\sqrt{2(1-\sin\theta\sin\phi)}} \\
&\overrightarrow{n} \cdot \overrightarrow{E}_i \\
&\quad = \frac{-E_{ix}\sin\theta\cos\phi - E_{iz}\cos\theta}{\sqrt{2(1-\sin\theta\sin\phi)}}.
\end{aligned}
\tag{23}
$$

APPENDIX II

PROOF OF THE STATEMENT THAT ERROR PROBABILITY IS INDEPENDENT OF THE ORIENTATIONS OF THREE ORTHOGONAL RECEIVE ANTENNAS

It is first assumed that three mutually orthogonal antennas are at the MS, and their orientation vectors are $\overrightarrow{l}_m = l_{mx}\overrightarrow{i}_x + l_{my}\overrightarrow{i}_y + l_{mz}\overrightarrow{i}_z, \quad m = 1, 2, 3$. In case of a single transmit antenna ($K = 1$), the corresponding channel correlation matrix is $\mathbf{R} = E[\boldsymbol{h}\boldsymbol{h}^H]$, where $\boldsymbol{h} = [H_1^1, H_2^1, H_3^1]^T$ is the channel coefficient vector whose elements are specified in (13), and the elements of $\mathbf{R}$ are specified by (16)

$$\begin{aligned}[\mathbf{R}]_{mm'} &= E\left[H_m^1 H_{m'}^{1*}\right] \\ &= E_\Omega\left[\left(\overrightarrow{g}_r^1 \cdot \overrightarrow{l}_m\right)\left(\overrightarrow{g}_r^1 \cdot \overrightarrow{l}_{m'}\right)\right] \end{aligned} \tag{26}$$

where $E_\Omega[\cdot]$ is used to denote the integral over Ω to simplify the notation. Meanwhile, the polarization vector of the reflected field is $\overrightarrow{g}_r^1 = g_{rx}^1\overrightarrow{i}_x + g_{ry}^1\overrightarrow{i}_y + g_{rz}^1\overrightarrow{i}_z$. The channel correlation matrix now becomes

$$\mathbf{R} = E_\Omega[\boldsymbol{V}\boldsymbol{V}^T] = \mathbf{L}E_\Omega\left[\boldsymbol{G}_1\boldsymbol{G}_1^T\right]\mathbf{L}^T \tag{27}$$

where

$$\boldsymbol{V} = \begin{bmatrix} \overrightarrow{g}_r^1 \cdot \overrightarrow{l}_1 \\ \overrightarrow{g}_r^1 \cdot \overrightarrow{l}_2 \\ \overrightarrow{g}_r^1 \cdot \overrightarrow{l}_3 \end{bmatrix} = \begin{bmatrix} l_{1x} & l_{1y} & l_{1z} \\ l_{2x} & l_{2y} & l_{2z} \\ l_{3x} & l_{3y} & l_{3z} \end{bmatrix} \begin{bmatrix} g_{rx}^1 \\ g_{ry}^1 \\ g_{rz}^1 \end{bmatrix} \triangleq \mathbf{L}\boldsymbol{G}_1.$$

It can be shown that $\mathbf{L}$ is a unitary matrix, and, consequently, $\mathbf{R}$ and $E_\Omega[\boldsymbol{G}_1\boldsymbol{G}_1^T]$ in (27) have the same set of eigenvalues. The eigenvalues of $\mathbf{R}$ remain the same for different orthogonal sets of $\{\overrightarrow{l}_1, \overrightarrow{l}_2, \overrightarrow{l}_3\}$, and the resultant P_e is thus independent of the orientations of the threebranch orthogonal structure. By modifying $\boldsymbol{h}$ properly, the proof can be extended to the case of more than one transmit antenna.

APPENDIX III

PROOF OF THE STATEMENT THAT ERROR PROBABILITY IS INDEPENDENT OF THE ROTATIONS OF TWO ORTHOGONAL TRANSMIT ANTENNAS

First of all, the polarization vector of the reflected field $\overrightarrow{g}_r$ defined in (6) can be simplified to

$$\begin{aligned}\overrightarrow{g}_r &= (\eta_x f_{x1} + \sqrt{1-\eta_x} f_{x2})\overrightarrow{i}_x \\ &\quad + (\eta_x f_{y1} + \sqrt{1-\eta_x} f_{y2})\overrightarrow{i}_y \\ &\quad + (\eta_x f_{z1} + \sqrt{1-\eta_x} f_{z2})\overrightarrow{i}_z \\ &= (\overrightarrow{g}_t \cdot \overrightarrow{F}_x)\overrightarrow{i}_x + (\overrightarrow{g}_t \cdot \overrightarrow{F}_y)\overrightarrow{i}_y + (\overrightarrow{g}_t \cdot \overrightarrow{F}_z)\overrightarrow{i}_z \end{aligned} \tag{28}$$

where f_{a1} and f_{a2} for $a = x, y, z$ are functions of k_ϵ, θ, and ϕ, $\overrightarrow{F}_a \triangleq f_{a1}\overrightarrow{i}_x + f_{a2}\overrightarrow{i}_z$ is also a function of those variables, and $\overrightarrow{g}_t$ is defined in (3). We first consider the case when only one receive antenna is at the MS with orientation vector $\overrightarrow{l}_1$, and two transmit antennas are at the BS with orthogonal transmit

$$\begin{aligned} & r_s[\overrightarrow{n} \cdot (\overrightarrow{a}_i \times \overrightarrow{E}_i)] \cdot (\overrightarrow{n} \times \overrightarrow{a}_i) \\ &\quad = \frac{r_s(E_{ix}\cos^2\theta - E_{iz}\sin\theta\cos\theta\cos\phi)}{2(1-\sin\theta\sin\phi)}\overrightarrow{i}_x \\ &\quad + \frac{r_s(E_{iz}\sin^2\theta\cos^2\phi - E_{ix}\sin\theta\cos\theta\cos\phi)}{2(1-\sin\theta\sin\phi)}\overrightarrow{i}_z \\ & r_l(\overrightarrow{n} \cdot \overrightarrow{E}_i)(\cos\theta_i\overrightarrow{a}_i + \cos 2\theta_i\overrightarrow{n}) \\ &\quad = \frac{r_l(-E_{ix}\sin^3\theta\cos^2\phi\sin\phi - E_{iz}\sin^2\theta\cos\theta\sin\phi\cos\phi)}{2(1-\sin\theta\sin\phi)}\overrightarrow{i}_x \\ &\quad + \frac{r_l(E_{ix}\sin\theta\cos\phi + E_{iz}\cos\theta - E_{ix}\sin^3\theta\sin^2\phi\cos\phi - E_{iz}\sin^2\theta\cos\theta\sin^2\phi)}{2(1-\sin\theta\sin\phi)}\overrightarrow{i}_y \\ &\quad + \frac{r_l(-E_{ix}\sin^2\theta\cos\theta\sin\phi\cos\phi - E_{iz}\sin\theta\cos^2\theta\sin\phi)}{2(1-\sin\theta\sin\phi)}\overrightarrow{i}_z. \end{aligned} \tag{24}$$

$$\begin{aligned} \overrightarrow{E}_r &= \frac{r_s(E_{ix}\cos^2\theta - E_{iz}\sin\theta\cos\theta\cos\phi) + r_l(E_{ix}\sin^3\theta\cos^2\phi\sin\phi + E_{iz}\sin^2\theta\cos\theta\sin\phi\cos\phi)}{1-\sin^2\theta\sin^2\phi}\overrightarrow{i}_x \\ &\quad + \frac{r_l(E_{ix}\sin^3\theta\sin^2\phi\cos\phi + E_{iz}\sin^2\theta\cos\theta\sin^2\phi - E_{ix}\sin\theta\cos\phi - E_{iz}\cos\theta)}{1-\sin^2\theta\sin^2\phi}\overrightarrow{i}_y \\ &\quad + \frac{r_s(E_{iz}\sin^2\theta\cos^2\phi - E_{ix}\sin\theta\cos\theta\cos\phi) + r_l(E_{ix}\sin^2\theta\cos\theta\sin\phi\cos\phi + E_{iz}\sin\theta\cos^2\theta\sin\phi)}{1-\sin^2\theta\sin^2\phi}\overrightarrow{i}_z. \end{aligned} \tag{25}$$

polarization directions $\overrightarrow{g}_t^1$ and $\overrightarrow{g}_t^2$. According to (28), we have

$$\begin{aligned}\overrightarrow{g}_r^k \cdot \overrightarrow{l}_1 &= (\overrightarrow{g}_t^k \cdot \overrightarrow{F}_x) l_{1x} + (\overrightarrow{g}_t^k \cdot \overrightarrow{F}_y) l_{1y} + (\overrightarrow{g}_t^k \cdot \overrightarrow{F}_z) l_{1z} \\ &= \overrightarrow{g}_t^k \cdot (\overrightarrow{F}_x l_{1x} + \overrightarrow{F}_y l_{1y} + \overrightarrow{F}_z l_{1z}) \triangleq \overrightarrow{g}_t^k \cdot \overrightarrow{q}_1 \quad (29)\end{aligned}$$

where $\overrightarrow{g}_r^k$ is the polarization vector of the reflected field corresponding to $\overrightarrow{g}_t^k$ for $k = 1$ and 2. Since the $\overrightarrow{F}_a$ defined above does not contain $\overrightarrow{i}_y$ component, $\overrightarrow{q}_1$ in (29) actually lies in the plane perpendicular to $\overrightarrow{i}_y$ and, hence, can be simplified to $\overrightarrow{q}_1 = q_{1x}\overrightarrow{i}_x + q_{1z}\overrightarrow{i}_z$. Furthermore, the channel vector in this case is $\boldsymbol{h} = [H_1^1, H_1^2]^T$ whose elements are specified in (13). Similar to (27), the corresponding correlation matrix is given by

$$\mathbf{R} = E[\boldsymbol{h}\boldsymbol{h}^H] = E_\Omega[\boldsymbol{V}\boldsymbol{V}^T] \quad (30)$$

where

$$\begin{aligned}\boldsymbol{V} &= \begin{bmatrix} \overrightarrow{g}_r^1 \cdot \overrightarrow{l}_1 \\ \overrightarrow{g}_r^2 \cdot \overrightarrow{l}_1 \end{bmatrix} = \begin{bmatrix} \overrightarrow{g}_t^1 \cdot \overrightarrow{q}_1 \\ \overrightarrow{g}_t^2 \cdot \overrightarrow{q}_1 \end{bmatrix} \\ &= \begin{bmatrix} g_{tx}^1 & g_{tz}^1 \\ g_{tx}^2 & g_{tz}^2 \end{bmatrix} \begin{bmatrix} q_{1x} \\ q_{1z} \end{bmatrix} \triangleq \mathbf{B}\boldsymbol{Q}_1.\end{aligned}$$

Consequently, the correlation matrix can be rewritten as

$$\mathbf{R} = \mathbf{B} E_\Omega \left[\boldsymbol{Q}_1 \boldsymbol{Q}_1^T\right] \mathbf{B}^T. \quad (31)$$

It can be easily shown that $\mathbf{B}$ is unitary and, therefore, the eigenvalues of $\mathbf{R}$ are independent of the two orthogonal directions $\overrightarrow{g}_t^1$ and $\overrightarrow{g}_t^2$. In case of two receive antennas, $\boldsymbol{V}$ in (30) will take the form

$$\begin{aligned}\boldsymbol{V} &= \left[\overrightarrow{g}_r^1 \cdot \overrightarrow{l}_1, \overrightarrow{g}_r^2 \cdot \overrightarrow{l}_1, \overrightarrow{g}_r^1 \cdot \overrightarrow{l}_2, \overrightarrow{g}_r^2 \cdot \overrightarrow{l}_2\right]^T \\ &= \begin{bmatrix} \mathbf{B} & \mathbf{0} \\ \mathbf{0} & \mathbf{B} \end{bmatrix} \begin{bmatrix} \boldsymbol{Q}_1 \\ \boldsymbol{Q}_2 \end{bmatrix} \triangleq \mathbf{B}_d \boldsymbol{Q}_d.\end{aligned}$$

Since $\mathbf{B}_d$ is still unitary, the eigenvalues of the correlation matrix are again independent of $\overrightarrow{g}_t^1$ and $\overrightarrow{g}_t^2$. Similarly, the proof can be extended to any number of receive antennas.

REFERENCES

[1] V. A. Fock, *Electromagnetic Diffraction and Propagation Problems*. New York: Pergamon, 1965.

[2] R. H. Clark, "A statistics theory for mobile radio," *Bell Syst. Tech. J.*, vol. 44, pp. 957–1000, 1972.

[3] W. C. Y. Lee and Y. S. Yeh, "Polarization diversity system for mobile radio," *IEEE Trans. Commun.*, vol. COM-22, pp. 912–923, Oct. 1972.

[4] W. C. Jakes, *Microwave Mobile Communications*. New York: Wiley, 1974.

[5] W. C. Y. Lee, *Mobile Communications Engineering*. New York: Wiley, 1982.

[6] S. Kozono, T. Tsuruhara, and M. Sakamoto, "Base station polarization diversity reception for mobile radio," *IEEE Trans. Veh. Technol.*, vol. VT-33, pp. 301–306, Nov. 1984.

[7] C. A. Balanis, *Advanced Engineering Electromagnetics*. New York: Wiley, 1989.

[8] H. Kuboyama, Y. Tanaka, K. Sato, K. Fujimoto, and K. Hirasawa, "Experimental results with mobile antennas having cross-polarization components in urban and rural areas," *IEEE Trans. Veh. Technol.*, vol. 39, no. 2, pp. 150–160, May 1990.

[9] R. G. Vaughan, "Polarization diversity in mobile communications," *IEEE Trans. Veh. Technol.*, vol. 39, no. 3, pp. 177–186, Aug. 1990.

[10] J. F. Lemieux, M. S. El-Tanany, and H. M. Hafez, "Experimental evaluation of space/frequency/polarization diversity in the indoor wireless channel," *IEEE Trans. Veh. Technol.*, vol. 40, no. 3, pp. 569–574, Aug. 1991.

[11] F. Chatelin, *Eigenvalues of Matrices*. New York: Wiley, 1993.

[12] J. G. Proakis, *Digital Communications*. New York: McGraw-Hill, 1995.

[13] A. M. D. Turkmani, A. A. Arowojolu, P. A. Jefford, and C. J. Kellett, "An experimental evaluation of the performance of two-branch space and polarization diversity schemes at 1800 MHz," *IEEE Trans. Veh. Technol.*, vol. 44, no. 2, pp. 318–326, May 1995.

[14] O. Landron, M. J. Feuerstein, and T. S. Rappaport, "A comparison of theoretical and empirical reflection coefficients for typical exterior wall surfaces in a mobile radio environment," *IEEE Trans. Antennas Propag.*, vol. 44, no. 3, pp. 341–351, Mar. 1996.

[15] J. C. Liberti and T. S. Rappaport, "A geometrically based model for line-of-sight multipath radio channels," in *Proc. IEEE 46th Vehicular Technology Conf.*, vol. 2, 1996, pp. 844–848.

[16] K. Kagoshima, K. Uehara, and T. Hori, "A miniaturized dual polarization antenna for a small wireless terminal," in *Proc. IEEE Antennas Propagation Society Int. Symp.*, vol. 2, Jul. 1996, pp. 1092–1095.

[17] G. J. Foschini and M. J. Gans, "On the limits of wireless communications in a fading environment when using multiple antennas," *Wireless Pers. Commun*, vol. 6, no. 3, pp. 311–335, Mar. 1998.

[18] T. Fulghum and K. Molnar, "The Jakes fading model incorporating angular spread for a disk of scatterers," in *Proc. IEEE 48th Vehicular Technology Conf.*, vol. 1, May 1998, pp. 489–493.

[19] X. J. A. Lempiainen and J. K. Laiho-Steffens, "The performance of polarization diversity schemes at a base station in small/micro cells at 1800 MHz," *IEEE Trans. Veh. Technol.*, vol. 47, no. 3, pp. 1087–1092, Aug. 1998.

[20] E. I. Teletar and D. Tse, "Capacity and mutual informantion of broad-band multipath fading channels," in *Proc. IEEE Int. Symp. Information Theory*, 1998, p. 188.

[21] L. M. A. Jalloul, K. Rohani, K. Kuchi, and J. Chen, "Performance analysis of CDMA transmit diversity methods," in *Proc. IEEE 50th Vehicular Technology Conf.*, vol. 2, Sep. 1999, pp. 1326–1330.

[22] R. B. Ertel and J. H. Reed, "Angle and time of arrival statistics for circular and elliptical scattering models," *IEEE J. Sel. Areas Commun.*, vol. 17, no. 11, pp. 1829–1840, Nov. 1999.

[23] D. Shiu, G. J. Foschini, M. J. Gans, and J. M. Kahn, "Fading correlation and its effect on the capacity of multielement antenna systems," *IEEE Trans. Commun.*, vol. 48, no. 3, pp. 502–513, Mar. 2000.

[24] T. Svantesson, "A study of polarization diversity using an electromagnetic spatio-temporal channel model," in *Proc. IEEE 52nd Vehicular Technology Conf.*, vol. 1, 2000, pp. 79–86.

[25] K. Atanassov, R. M. Narayanan, V. Stoiljkovic, and G. R. Kadambi, "Mobile station polarization diversity reception for handheld devices at 1.8 GHz," in *Proc. IEEE Antennas and Propagation Society Int. Symp.*, vol. 1, 2000, pp. 290–293.

[26] C. D. Meyer, *Matrix Analysis and Applied Linear Algebra*. Philadelphia, PA: SIAM, 2000.

[27] T. Svantesson, "A physical MIMO radio channel model for multi-element multi-polarized antenna system," in *Proc. IEEE 54th Vehicular Technology Conf.*, vol. 2, 2001, pp. 1083–1087.

[28] L. Lukama, K. Konstantinou, and D. J. Edwards, "Polarization diversity performance for UMTS," in *Proc. 11th Int. Conf. Antennas and Propagation*, vol. 1, 2001, pp. 193–197.

[29] L. C. Lukama, K. Konstantinou, and D. J. Edwards, "Performance of a three-branch orthogonal polarization diversity scheme," in *Proc. IEEE 54th Vehicular Technology Conf.*, vol. 4, 2001, pp. 2033–2037.

[30] C. C. Martin, J. H. Winters, and N. R. Sollenberger, "Multiple-input multiple-output (MIMO) radio channel measurements," in *Proc. IEEE Antennas and Propagation Society Int. Symp.*, vol. 1, Jul. 2001, pp. 418–421.

[31] S. H. Simon, A. L. Molisch, M. Stoytchev, and H. Safar, "Communication in a disordered world," *Physics Today*, vol. 54, Sep. 2001.

[32] X. F. Dong and N. C. Beaulieu, "Average level crossing rate and fade duration of maximal ratio diversity in unbalanced and correlated channels,"

in *Proc. IEEE Wireless Communications and Networking Conf.*, vol. 2, Mar. 2002, pp. 762–767.

[33] R. U. Nabar, H. Bolcskei, V. Erceg, D. Gesber, and A. J. Paulraj, "Performance of multiantenna signaling techniques in the presence of polarization diversity," *IEEE Trans. Signal Process.*, vol. 50, no. 10, pp. 2553–2562, Oct. 2002.

[34] C. Yu, B. Z. Wang, and W. X. Wu, "A compact planar polarization diversity antenna for mobile communication," in *Proc. IEEE Antennas and Propagation Society Int. Symp.*, vol. 3, Jun. 2003, pp. 682–685.

[35] K. R. Dandekar, S. Kawale, R. W. Heath Jr., and L. Dong, "Electromagnetic characterization of MIMO communication systems," *IEEE Trans. Veh. Technol.,* submitted for publication.

[36] J. W. Wallace and M. A. Jensen, "The capacity of MIMO wireless systems with mutual coupling," in *Proc. IEEE 56th Vehicular Technology Conf.*, vol. 2, 2002, pp. 696–700.

[37] L. Dong, H. Choo, H. Ling, and R. W. Heath Jr., "Simulation of MIMO channel capacity with antenna polarization diversity," *IEEE Trans. Wireless Commun.,* submitted for publication.

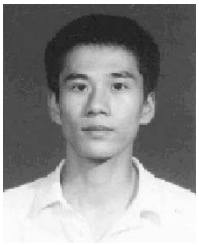

Yan Zhou (S'00) received the B.E. degree in communications engineering from Beijing University of Posts and Telecommunications, Beijing, China, in 1997 and the Master degree from National University of Singapore, Singapore, in 2001. Since 2002, he has been pursuing the Ph.D. degree at the University of Wisconsin-Madison. His research interests include wide-band CDMA systems, smart antennas, power control, and multimedia multirate transmission.

Akbar M. Sayeed (S'89–M'97–SM'02) received the B.S. degree from the University of Wisconsin–Madison, in 1991 and the M.S. and Ph.D. degrees in 1993 and 1996, respectively, from the University of Illinois at Urbana-Champaign, all in electrical and computer engineering.

From 1991 to 1996, he was a research assistant with the Coordinated Science Laboratory, University of Illinois. From 1996 to 1997, he was a postdoctoral fellow at Rice University, Houston, TX. Since August 1997, he has been with the University of Wisconsin–Madison, where he is currently Associate Professor of electrical and computer engineering. His research interests are in wireless communications, statistical signal processing, information theory, time-frequency analyis, and applications in networks.

Dr. Sayeed received a Schlumberger Fellowship from 1992 to 1995 and the Robert T. Chien Memorial Award in 1996 for his doctoral research at the University of Illinois. He received the NSF CAREER Award in 1999, the ONR Young Investigator Award in 2001, and a University of Wisconsin Grainger Junior Faculty Fellowship in 2003. He served as an Associate Editor for the IEEE SIGNAL PROCESSING LETTERS from 1999 to 2002 and as a co-guest editor in 2004 for a special issue of the IEEE JOURNAL ON SELECTED AREAS IN COMMUNICATIONS on Self-Organizing Distributed Collaborative Sensor Networks.